

Low Profile UHF/VHF Metamaterial Backed Circularly Polarized Antenna Structure

Taulant Rexhepi^{1, *}, Igor Bendoy², Ada-Simona Popescu¹, Andrii Golovin¹, Johnny Daniel³, Kate J. Duncan³, and David Crouse²

Abstract—In this work, a low-profile metamaterial backed planar antenna structure designed to work in the UHF/VHF range is presented. The antenna has right-hand circular polarization. It is ideal for satellite-based communications and radar systems. An artificial magnetic conductor was designed using a metamaterial composed of a split ring resonators to reduce the size of the planar antenna and ground plane system. The proposed artificial magnetic conductor has more confined surface waves at the reflecting plane than previous designs and is suitable for circular polarization. Through numerical simulations, performance characteristics including return-loss, and realized gain of the antenna systems are calculated and analyzed in the VHF range. The proposed antenna system is narrowband and is linearly scalable in the range of 100 MHz–1 GHz.

1. INTRODUCTION

Over the recent decade, a major area of interest for microwave researchers has been the replacement of metallic electric-conducting ground planes of antennas with artificial magnetic material surfaces made from metamaterials [1–7]. With such structures, it was demonstrated that the distance between the antenna and the metal ground plane can be significantly reduced while maintaining the optimized gain [2].

The radiation emitted by a planar antenna has two components: a forward propagating component emitted in the direction of the receiver or target, and a backwards propagating component that, unless captured, would be wasted. Antennas typically use metal ground planes to capture this second component of the signal. However, the ground plane must be placed at a particular distance away from the antenna to ensure that the backwards propagating component after being reflected constructively interferes with the forward propagating component, thereby increasing the gain of the system by 3 dB [8]. With the $\sim 180^\circ$ phase change that an electromagnetic beam undergoes upon reflection from a metal, the minimum antenna-ground plane separation distance is $\lambda/4$ when the ground plane is a metal [8].

This requirement of a $\lambda/4$ separation between the emitting element and standard metallic ground plane becomes problematic when one needs to design compact lightweight antennas. It is also highly desired in applications such as GPS and SATCOM communications that the antenna is circularly polarized, hence special consideration has to be made for the ground plane to ensure that the circular polarization of the antenna is maintained upon reflection off the ground plane.

With metamaterial ground planes that mimic Artificial Magnetic Conductors (AMCs), the phase change of the beam upon reflection can be made $\sim 0^\circ$ over a certain frequency bandwidth. This allows the antenna-ground plane separation to be close to zero for that frequency band. The first generation

Received 9 September 2015, Accepted 16 November 2015, Scheduled 23 November 2015

* Corresponding author: Taulant Rexhepi (trexhep00@cuny.cuny.edu).

¹ Electrical Engineering Department, City College, The City University of New York, 160 Convent ave, New York, NY 100310, USA. ² Phoebus Optoelectronics LLC, New York, USA. ³ US Army, Weapons and Materials Research Directorate, Aberdeen Proving Grounds, MD 21005, USA.

of AMC arrays described in [1–4], consisted of an array of square patches connected through via holes to the ground plane to prevent the excitation of surface waves. This configuration came to be known as the mushroom structure. These structures work well for circularly polarized antennas in the higher RF spectrum, however when applied to antenna systems in the UHF/VHF band, the structures become problematic to fabricate. The AMC presented in this work is easier to fabricate since it does not require any via-holes and shows better performance, in terms of surface wave excitation.

2. GEOMETRY OF THE ANTENNA

Planar antennas have attracted the attention of many researchers and industry engineers in the recent years due to the ease of the fabrication. There is an increasing demand for both military and industry applications for low profile, compact size, conformal and circularly polarized antennas. Another attractive feature of planar antennas is the fact that they can be fabricated with standard printed circuit board (PCB) manufacturing methods that allow for a wide variety of geometric shapes [5–8]. Together with a ground plane, these planar antennas can provide very good directivity [9]. For applications in the higher RF spectrum, namely the S-X bands, they are also very compact in size, however for the lower frequencies they are bulkier, which depending on the application can be problematic. The main focus of this work is the design and performance of the AMC surface and not the primary radiator. In spite of this, care was taken to optimize the geometry of the antenna such that it has a well-defined gain in the frequency range of interest.

The antenna described here is a four clover shaped planar antenna, (Figure 1(a)). The clover or teardrop shape has been widely used, particularly for broadband technologies in wireless communications [7, 8]. Concerning the physical dimensions of the structures in this work (i.e., antenna and metamaterial ground plane), all results are normalized relative to the lowest frequency f_0 . Depending on the desired operating frequency, all structural dimensions of the primary radiator are given in terms of the operating wavelength, λ_C and can be scaled identically using the same scale factor that scales the operating frequency, f_C . Good performance of the antenna is maintained for scaling factors that yield f_C values in the range of 100 MHz–1 GHz. The bandwidth of the antenna system is primarily dictated by the bandwidth of the AMC structure which also scales well with frequency. The substrate for the antenna is $\lambda/1000$ thick with a dielectric constant value of 2.17 and loss tangent of 0.0008. Being that the antenna is a cross-dipole, its gain in free space (i.e., no ground plane) is

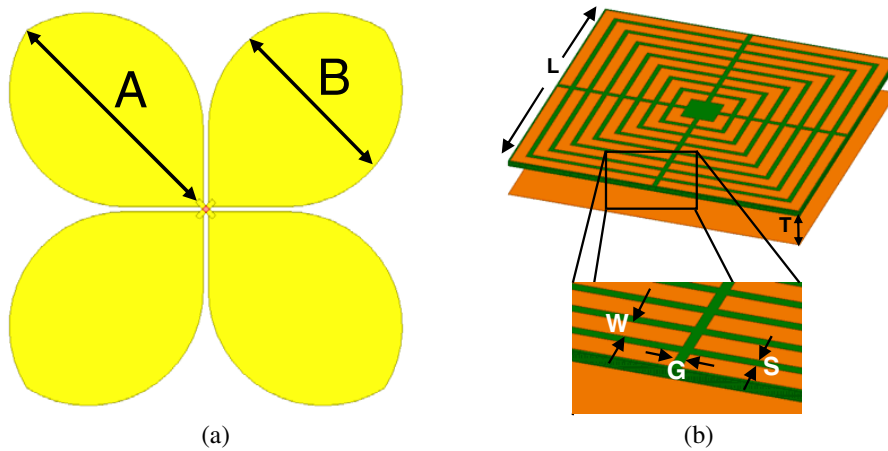


Figure 1. (a) Geometry of the four clover shaped planar antenna: dimensions $A = \lambda/5$ and $B = \lambda/7$. The feed of the antenna is the small crisscrossing structure in the middle, all four clovers are same dimensions and rotated 90° . (b) The geometry of the SRR unit cell, the dimensions are based on the wavelength, λ of the resonant frequency, f_R as follows: $L = \lambda/6.25$, $S = G = \lambda/2000$, $T = \lambda/48$, and $W = \lambda/110$. The dielectric thickness is on the order of $\lambda/315$. The separation between adjacent rings is $\lambda/2000$ on all four sides.

around 2.5 dB. The metal reflector adds another 3 dB in the direction of desired gain increase. Further optimizations techniques, such as employing the clover design and rounding sharp edges add another 2 dB making the total gain at boresight roughly 7 dB.

3. ARTIFICIAL MAGNETIC CONDUCTOR SURFACE

AMCs can be of various configurations. The most widely used is the mushroom structure which consists of square patches interconnected to a metallic ground plane. Another way of implementing such a system is by using two layers; the top layer consisting of a capacitive array which would not be connected to the ground plane. In this form the top layer consists of an array of periodic elements with lateral dimensions on the order of $\lambda/10$ [10, 11]. The characteristics of AMCs are dictated by the geometries, orientations and configurations of the metal and dielectric structures of which they are composed; such characteristics and their dependencies have been the focus of many research efforts in the microwave field in recent years [1–4, 10, 11]. In this work, the Split Ring Resonator (SRR) was chosen as the unit cell of the AMC. While different in important ways than previously reported AMCs based on splitting resonators (SRRs) [10–15], the resulting AMC described in this work (Figure 1(b)) still uses this important structure as its key component. AMCs based on SRRs have been used as an innovative method for reducing the overall thickness of planar antennas [11–14]. In [16], Ayed et al. demonstrated that this method can be used to reduce the profile of a simple linearly polarized dipole antenna. In their work, SRRs were also chosen over the conventional square patches. It is important to note that in this configuration the magnetic moment of the SRR is not being excited, the geometry serves to provide mainly capacitance. Other similar works have also used SRRs for antenna systems [12, 14, 16], however the applications were limited to linearly polarized antennas. Mushroom structures have been shown to work well with circularly polarized antennas for GPS applications in the L band [17, 18]. To the best of our knowledge, no previous research has been reported describing SRR AMCs operating in the VHF band for circularly polarized antennas. Our work described in his paper verifies that such structures work well in VHF and UHF antenna systems.

The unit cell of the AMC given in Figure 1(b) was based on the work done by [19]. The dimensions of the unit cell are presented in terms of the wavelength, λ corresponding to the resonant frequency, f_R of the AMC. Good performance of the AMC is maintained for scaling factors that yield f_R values in the range of 100 MHz–1 GHz. The fractional bandwidth of the AMC is maintained through this given range. In this design the substrate that was used was the Rogers TTM13i dielectric ($\epsilon_R = 12.2$).

The behavior of AMCs is analogous to an RLC transmission line, in which the three lumped elements are in parallel. The capacitance and inductance of the AMC are dependent on geometric shape and size of the unit cell. Capacitance is produced by the gaps in the pattern as can be seen in Figure 2(a) by the concentration of the electric fields between the metal strips. The high electric field intensities (which yield a high capacitance) are mainly concentrated in the splits of the outer most rings. Thus, the four outer-most rings have the most influence in the capacitance of the AMC. The inner four rings have only a slight impact in the resonant frequency, with the rings providing additional capacitance and inductance such that the resonant frequency can be achieved with the smallest possible dimensions. Capacitance can be further increased by decreasing the spacing between adjacent unit cells, which would further decrease the lateral dimensions; however it would make tuning the structure more complex.

The inductance of the system is primarily created from the capacitive array and ground plane combination as in the case of the classical AMC [1]. The incident radiation drives current along the copper strips, which creates a magnetic field around them, as shown in Figure 2(b). This also contributes to the inductance of the AMC; however, the contribution is very small and can be neglected. The inductance and capacitance create resonant conditions from which the useful properties of the AMC are drawn. Values of the capacitance of the structure can be approximated by using the method presented in [19]. The equivalent capacitance of the unit cell for the circuit model is given by [19]:

$$C = \frac{7}{4} [2L - (15)(W + S)] C_0 \quad (1)$$

where C_0 is the per-unit-length capacitance between two parallel strips having width W and separation

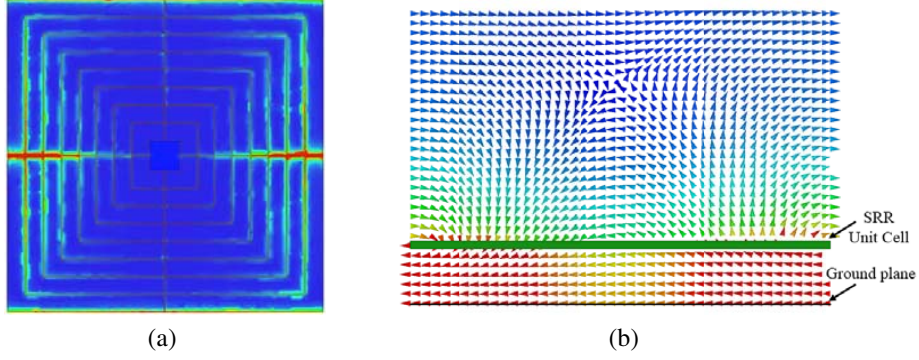


Figure 2. (a) Top view of SRR showing electric field magnitude on the plane of the SRR demonstrating the capacitance. (b) Side view of the SRR unit cell illustrating the intensified magnetic field region around the rings induced by the current given a normally incident plane wave with TE polarization.

S , given by:

$$C_0 = \varepsilon_0 \frac{K(\sqrt{1-k^2})}{K(k)} \quad (2)$$

with $K(k)$ being the elliptic integral of the first kind and

$$k = \frac{\frac{S}{W}}{W + \frac{S}{W}} \quad (3)$$

The equivalent inductance which depends mainly on the distance from the SRR array and the groundplane is approximated by:

$$L = T\mu_0 \quad (4)$$

The capacitance and inductance are also dependent on the polarization of the incident radiation. The unit cell of the array has to be properly designed such that the capacitance and inductance values are identical for both polarizations. Conventionally, this is achieved by making the structure four-fold symmetric [20], as done in the structure shown in Figure 1(b). The resonant frequency of the AMC is related to the capacitance and inductance of the system, as per the very well-known equation:

$$f_R = \frac{1}{2\pi\sqrt{LC}} \quad (5)$$

From this relation it can be seen that if the AMC is designed such that L and C are polarization independent, then the structure will resonate at the same frequency regardless of polarization. Since the AMC structure is backed by a metal conductor, the transmission line equivalent is a terminated line. The reactance of the equivalent parallel RLC circuit approximates the surface impedance of the AMC and is given by:

$$Z_{SRR} = \frac{(R_L + j\omega L) \left(R_C - \frac{j}{\omega C} \right)}{R_L + R_C + j \left(\omega L - \frac{1}{\omega C} \right)} \quad (6)$$

where the R 's encompasses the losses occurring in the resistive metal (R_L) and the absorbing dielectric (R_C). These values can be found analytically using the method described in [21]. The reflection coefficient is given by:

$$\Gamma = \frac{Z_{im} - Z_{re}}{Z_{im} + Z_{re}} \quad (7)$$

where Z_{re} and Z_{im} are the real and imaginary parts of the Z_{SRR} , respectively. The reflection phase of the system is dependent on the resistance and reactance of the line by the following equation:

$$\theta = \tan^{-1} \left[\frac{Z_L - Z_C}{R} \right] \tag{8}$$

At resonance, the reactance caused by the inductance (Z_L) and capacitance (Z_C) equal each other (Figure 4(a)). From Equation (8) we see that this (i.e., resonance) causes the phase of the reflected wave to pass through zero (Figure 4(b)). The surface impedance and phase of reflection are frequency dependent, as predicted by both the transmission line model and the full wave finite element method simulations. The design equations for the equivalent capacitance and inductance are accurate with a 6% variation at most, which occurs at the higher-end of the scaling band.

To characterize the surface wave excitation of the structure we plotted the Z-component of the electric field on a cut-plane near the reflecting surface of the AMC (Figure 3). The baseline for the comparison is the ‘mushroom’ variation of the AMC. Geometrical differences between the compared structures means that the two structures need to have different lateral dimensions to resonate at the same frequency. In order to have a valid comparison the spacing between the square patches and the ground plane was kept the same as the spacing between the SRR and the ground plane. Also the distance between two adjacent square patches was kept the same as the distance between two adjacent SRRs. Magnitude of the z-component of the electric field is shown in Figure 4. From visual inspection one can see that the surface waves in the mushroom array extend significantly further than that of the SRR array. Hence the surface waves are more confined in the SRR and they will not impede the radiation emitted from the cross-dipole as much as those emitted from the mushroom structure. Additionally the suspended transmission line model [22, 23] is used to determine the surface wave propagation across the two AMC structures. In this method the capacitive array of the AMC is inserted between an optimized microstrip and the groundplane. The microstrip is then excited by two 50-ohm ports at the ends which allows one to efficiently characterize the AMC surfaces in terms of surface wave propagation [23]. Surface wave suppression is evident in Figure 3(b) for both of the AMC structures at the resonant frequency. The SRR based AMC does exhibit 50% less surface wave excitation which is evident by the -3 dB difference from the mushroom based AMC. One can also notice that the bandwidth of the mushroom structure is slightly wider than that of the SRR which is a result of the increased inductance caused by the vias in the middle of patch.

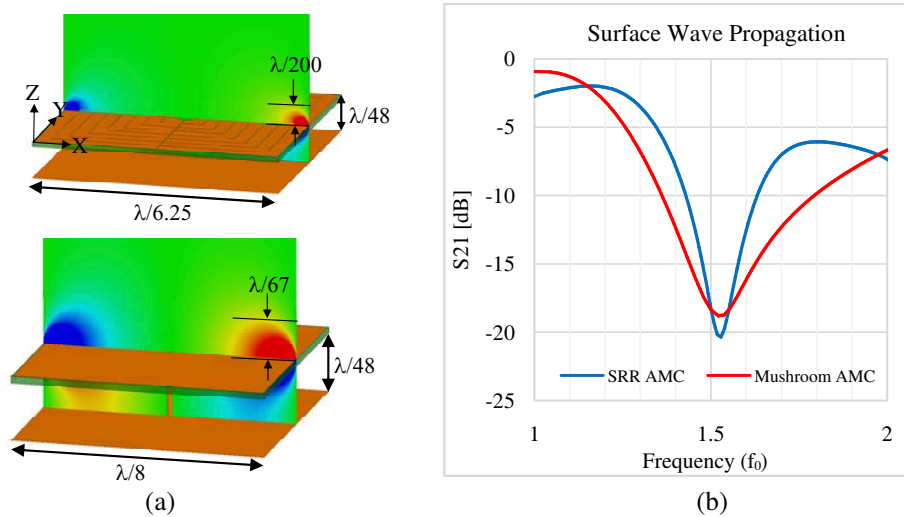


Figure 3. (a) Normalized surface wave excitation on SRR unit cell (top), and mushroom structure unit cell (bottom) given a normally incident plane wave at resonant frequency and polarized in the X direction. These results demonstrate that the SRR structure experiences less surface wave excitation than the mushroom based AMC. (b) Plot showing surface wave propagation using suspended transmission line method.

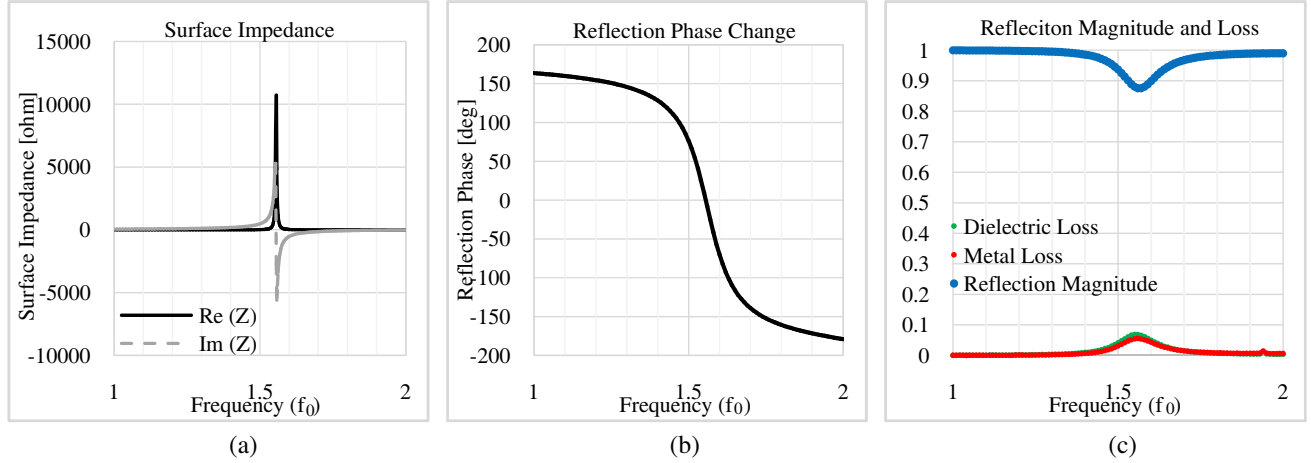


Figure 4. (a) Simulated surface impedance of the AMC. This impedance profile is analogous to that of a series resonant RLC. The plot can be found analytically by using Equation (6). (b) The simulated reflection phase of the AMC structure using HFSS, the resonant frequency is slightly passed $1.5f_0$. The reflection phase is identical for both polarizations. (c) Reflection magnitude and loss of AMC unit cell. The loss was calculated using volume loss density in the AMC dielectric substrate and surface loss density in the all the copper in the AMC structure.

4. RESULTS

The surface impedance of the AMC is given in Figure 4(a), it follows the profile of its equivalent transmission line model. The phase of the reflection of the AMC array is shown in Figure 4(b). These results were obtained using HFSS, a full-wave finite element method (FEM) modeling program that is commercially available. One can also calculate the reflection magnitude by using the impedance profile and Equation (7). Likewise one can also use the impedance profile to obtain the reflection phase change (Figure 4(b)) with Equation (8). The loss in the AMC reflector was characterized using the volume and surface loss density. Figure 4(c) shows that the loss in the dielectric and the copper are comparable to each other, the loss in the dielectric peaks at 6.9% meanwhile for the copper it peaks at 5.5%. In order to ensure agreement of results, two types of simulations were performed: the unit cell was simulated with periodic boundary conditions, and subsequently, with perfect E and perfect H boundary conditions at the sides of the unit cells. The two methods produced identical results due to the symmetry of the structure. The AMC surface was simulated using two orthogonal polarizations to ensure that the structure was polarization independent.

From the results presented in Figures 4(a) and 4(b), we can see that the array will show identical behavior regardless of polarization. The bandwidth of the AMC array is defined as the frequency range over which the reflection phase falls between $+90^\circ$ and -90° [21]. The nature of resonant structures is such that they exhibit their unique properties within a very narrow band of frequencies. This often leads to loss of performance at frequencies outside the bandwidth of AMC. For the case of AMCs there exists a relation between the spacing between the SRR array plane and the metal ground plane, and the bandwidth of the structure [24]. Ideally, a large spacing would be able to achieve a high bandwidth which is desired for antennas in this frequency range. However, achieving a high bandwidth for the AMC structure is not limited to having a large spacing between the two planes. Varactor diodes can also be used to tune the resonant frequency of the structure over the operational bandwidth of the antenna [25]. The varactors add a slight complexity to the structure, requiring the use of a biasing network. When using varactors, the AMC array should be designed to resonate at the highest operating bandwidth. When biasing the varactors to increase capacitance, the operating frequency of the structure will thereby decrease, allowing for an increase operational bandwidth. Work is also being done with Negative Impedance Converter (NICs) circuits as an alternative to widen the operational bandwidth of the AMCs [26].

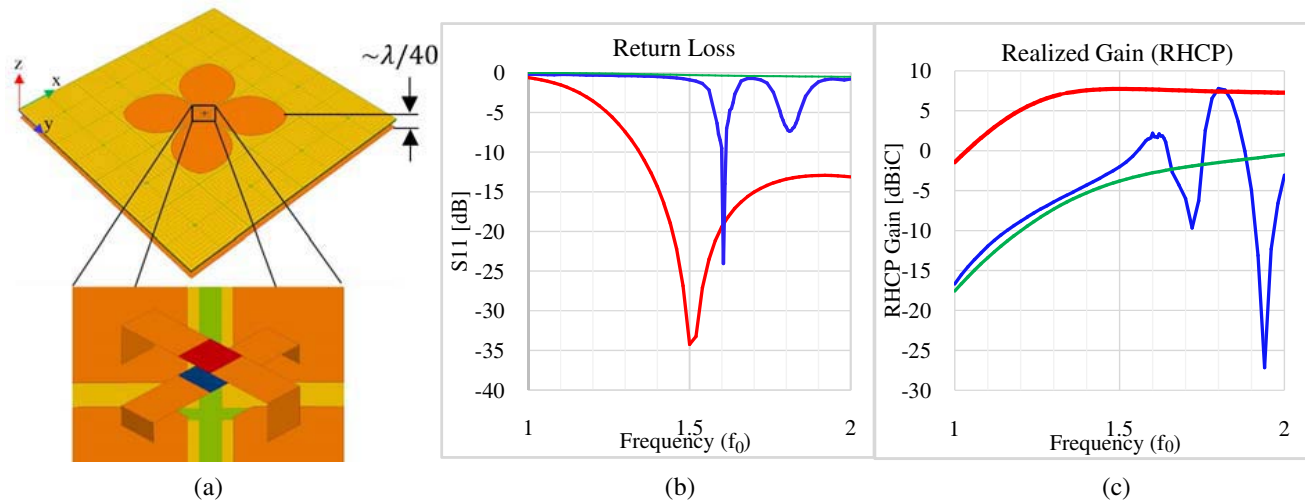


Figure 5. (a) Antenna backed by the AMC surface. With the AMC, the antenna can be placed at a distance of $\lambda/40$ away from the metal reflector, thus making the system much more compact than antenna systems that use solely metal ground planes. Details of the antenna feed. Two wave-port excitations (shown in blue and red) are fed with a phase difference of 90° . (b) Return loss, (c) realized RHCP gain at boresight as a function of frequency. The colors correspond to the following devices: antenna with classical air cavity and metal groundplane at $\lambda/4$ (red), antenna with AMC at $\lambda/40$ (blue), and antenna with air cavity and metal groundplane at $\lambda/40$ (green).

The AMC surface which is integrated in the antenna system contains an array of 4×4 SRRs. This corresponds to an aperture of $\lambda/1.5$ for the ground plane. The poles of the cross-dipole antenna line up with the diagonals of the AMC array (Figure 5(a)). The feed, as defined in the HFSS simulations, consisted of two wave-ports with an impedance of 50Ω , and with the two poles being fed 90° out of phase relative to each other. Such a feed delivers the desired circular polarization without the need of a balun. A detail of the antenna feed is given in Figure 5(a). To compare the system, three variations of the system were modeled: (1) an antenna separated from a metal ground plane by a distance of $\lambda/4$ serving as the baseline, (2) an antenna separated from an AMC ground plane by a distance of $\lambda/40$, and (3) an antenna separated from a metal ground plane by a distance of $\lambda/40$.

The simulation of the complete antenna system including the primary radiator and the AMC array contained 5.4 million tetrahedral mesh cells and was performed using domain decomposition and a high performance computing cluster. The results of the complete antenna system revealed that once the unit cell of the AMC no longer has infinite boundary conditions on the sides, the resonant frequency of the structure shifts towards a higher frequency. The change in this case is only 3% however since the bandwidth of the system is very narrow it is important to note. It should also be noted that in addition to the band around the resonance of the AMC, there is an additional band at a slightly higher frequency at which the antenna achieves its optimum gain, as shown in Figure 5(c). The existence of this higher band is caused by the finite size of the SRR array and groundplane. One can compensate for this increase in frequency by increasing the number of unit cells in the array which provides higher homogeneity [27]. Figure 5(b) shows the return loss measured at one of the wave-ports which fed the antenna; the other port was not included because it had near identical results. At the higher band which antenna performance is significantly improved, with the return loss being slightly above -10 dB. However, because the radiation does not create highly concentrated field regions as in the case of the resonance, and hence losses in the dielectric are minimized the realized gain is optimized. At the designed resonant frequency, the return loss goes well below -10 dB so the antenna can still be utilized efficiently at that band also.

We characterized the antenna performance by using numerical simulations. The realized RHCP gain of the antenna at boresight was plotted in terms of frequency. The results which are given in

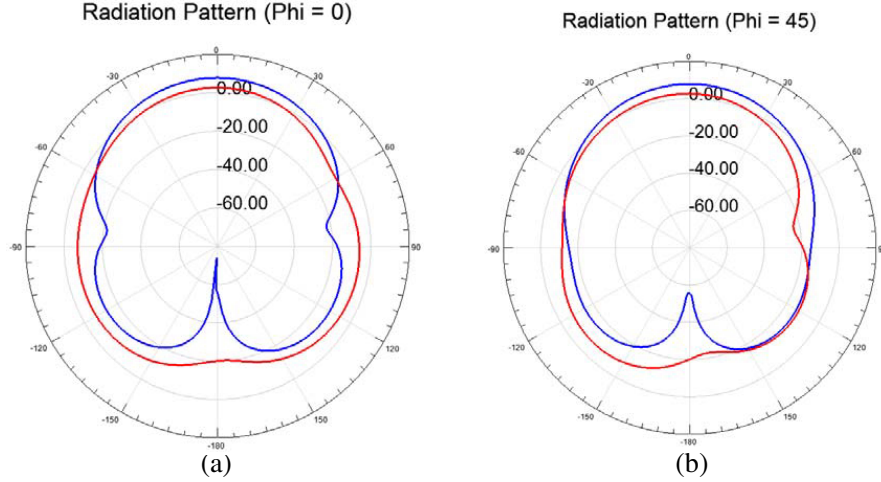


Figure 6. (a) Radiation pattern (realized RHCP gain) of the AMC based antenna system for $\phi = 0$, the red curve corresponds to the resonance of the AMC occurs, i.e., $f = f_R$, while the blue curve is the frequency where the gain is maximum at boresight, $f = 1.8f_0$. (b) Radiation pattern of the AMC based antenna system for $\phi = 45^\circ$, the red curve corresponds to the resonance of the AMC occurs, i.e., $f = f_R$, while the blue curve is the frequency where the gain is maximum at boresight, $f = 1.8f_0$.

Figure 5(c) include the antenna with a conventional metallic reflector for comparison purposes. At the resonant frequency of the AMC the gain of the antenna is only slightly increased. The AMC attains its characteristic behavior mainly at normal incidence. Once incidence angles greater than normal incidence are introduced the resonant frequency shifts significantly [28]. Having a low bandwidth then causes destructive interference for some angles which then drives down the realized gain at that frequency. Additionally, the losses in the metal and dielectric cause some of the radiation to be absorbed further reducing the realized gain. The optimal gain occurs at a slightly higher frequency where it slightly surpasses the gain of the antenna with plain metal reflector at $\lambda/4$.

The radiation patterns for the RHCP gain were plotted at the resonant frequency of the AMC and the frequency at which the maximum realized gain at boresight occurred. The patterns were calculated for $\phi = 0^\circ$, and $\phi = 45^\circ$ (Figures 6(a) and 6(b) respectively). The variation in the patterns for the different angles is caused by the geometry of the AMC reflector not being circular. This difference is most apparent at the side lobes of the pattern. For $\phi = 45^\circ$ the pattern exhibits some deformation in the back lobe which is caused by the ground plane being very close to the radiating element.

5. CONCLUSION

In this paper a low profile metamaterial enhanced antenna system designed to operate in the VHF/UHF range is presented. The antenna is circularly polarized. It was demonstrated by a full-wave finite element method computer simulations (HFSS) that the designed AMC structure is polarization independent and works well with circular polarization. Additionally we have shown that the surface waves can be further contained if a SRR geometry is used over the conventional square patches. The AMC allowed the overall profile of the antenna to be reduced by a factor of ~ 10 while maintaining the increased gain provided by the ground plane.

ACKNOWLEDGMENT

This work was supported by the NSF Industry/University Cooperative Research Center for Metamaterials (grant number IIP-1068028). The authors thank Hugh Carmichael for their help with HFSS simulations.

REFERENCES

1. Dan, S., et al., "High-impedance electromagnetic surfaces with a forbidden frequency band," *IEEE Trans. Microwave Theory and Tech.*, Vol. 47, No. 11, 2059–2074, 1999.
2. Sievenpiper, D. F., J. H. Schaffner, H. J. Song, R. Y. Loo, and G. Tansonan, "Two-dimensional beam steering using an electrically tunable impedance surface," *IEEE Trans. Antennas and Propagation*, Vol. 51, No. 10, 2713, 2722, 2003.
3. Broas, R. F. J., D. F. Sievenpiper, and E. Yablonovitch, "A high-impedance ground plane applied to a cellphone handset geometry," *IEEE Trans. Microwave Theory and Tech.*, Vol. 49, No. 7, 1262–1265, 2001.
4. Costa, F., et al., "An active high-impedance surface for low-profile tunable and steerable antennas," *IEEE Antennas and Wireless Propagation Letters*, Vol. 7, 676–680, 2008.
5. Suh, S.-Y., et al., "Evolution of broadband antennas from monopole disc to dual-polarized antenna," *IEEE Antennas and Propagation Society International Symposium*, 2006.
6. Liu, Y., et al., "A novel dual-polarized dipole antenna with compact size for wireless communication," *Progress In Electromagnetics Research*, Vol. 40, 217–227, 2013.
7. Suh, S.-Y., et al., "An novel broadband antenna, the low profile dipole planar inverted cone antenna (LPdiPICA)," *IEEE Antennas and Propagation Society International Symposium*, 2004.
8. Suh, S.-Y., et al., "A novel printed dual polarized broadband antenna-the fourclover antenna," *Proceedings of ISAP'04*, Sendai, Japan, 2004.
9. Balanis, C., *Antenna Theory, Analysis, and Design*, 2nd Edition, New Jersey, Wiley, USA, 2005.
10. Oh, S.-S. and L. Shafai, "Artificial magnetic conductor using split ring resonators and its applications to antennas," *Microwave and Optical Technology Letters*, Vol. 48, No. 2, 329–334, 2006.
11. Huang, Y., et al., "Enhancement of radiation along the ground plane from a horizontal dipole located close to it," *IEEE Antennas and Wireless Propagation Letters*, Vol. 7, 294–297, 2008.
12. Kärkkäinen, M. and P. Ikonen, "Patch antenna with stacked split-ring resonators as an artificial magneto-dielectric substrate," *Microwave and Optical Technology Letters*, Vol. 46, No. 6, 554–556, 2005.
13. Zhu, S., K. L. Ford, A. Tennant, and R. J. Langley, "SRR driven miniaturized dipole antenna with loaded AMC surface," *ESA Conference 2010*, [Online]. Available: <http://utopia.duth.gr/~iaitidis/ESA%20conference%202010/Papers/session%2011/FCXNL-10C09-1982541-1-1982541zhu.pdf>.
14. Erentok, A., P. L. Luljak, and R. W. Ziolkowski, "Characterization of a volumetric metamaterial realization of an artificial magnetic conductor for antenna applications," *IEEE Trans. Antennas and Propagation*, Vol. 53, No. 1, 160–172, 2005.
15. Sohn, J. R., K. Y. Kim, H.-S. Tae, and H. J. Lee, "Comparative study on various artificial magnetic conductors for low-profile antenna," *Progress In Electromagnetics Research*, Vol. 61, 27–37, 2006.
16. Ayad, H., et al., "Performances of low profile dipole antenna AMC-based surface using metamaterials structures," *2012 IEEE 19th International Conference on Telecommunications (ICT)*, 2012.
17. Baracco, J.-M., L. Salghetti-Drioli, and P. de Maagt, "AMC low profile wideband reference antenna for GPS and GALILEO systems," *IEEE Trans. Antennas and Propagation*, Vol. 56, No. 8, 2540–2547, 2008.
18. Carrubba, E., A. Monorchio, and G. Manara, "Artificial magnetic surface for circularly polarized antennas," *IEEE Antennas and Propagation Society International Symposium, 2009, APSURSI'09*, 1–4, 2009.
19. Bilotti, F., A. Toscano, and L. Vegni, "Design of spiral and multiple split-ring resonators for the realization of miniaturized metamaterial samples," *IEEE Trans. Antennas and Propagation*, Vol. 55, No. 8, 2258–2267, 2007.

20. Shen, X., et al., "Polarization-independent wide-angle triple-band metamaterial absorber," *Optics Express*, Vol. 19, No. 10, 9401–9407, 2011.
21. Costa, F., A. Monorchio, and G. Manara, "Analysis and design of ultra thin electromagnetic absorbers comprising resistively loaded high impedance surfaces," *IEEE Trans. Antennas and Propagation*, Vol. 58, No. 5, 1551–1558, 2010.
22. Dual-layer EBG structures for low profile bent antenna," *Progress In Electromagnetics Research B*, Vol. 47, 315–337, 2013.
23. Li, Y., et al., "A novel compact electromagnetic-bandgap (EBG) structure and its applications for microwave circuits," *IEEE Trans. Microwave Theory and Techniques*, Vol. 53, No. 1, 183–190, 2005.
24. Balanis, C., *Advanced Engineering, Electromagnetics, Analysis, and Design*, 2nd Edition, Wiley, USA, New York, 2012.
25. Costa, F., et al., "An active high-impedance surface for low-profile tunable and steerable antennas," *IEEE Antennas and Wireless Propagation Letters*, Vol. 7, 676–680, 2008.
26. Gregoire, D. J., C. R. White, and J. S. Colburn, "Wideband artificial magnetic conductors loaded with non-Foster negative inductors," *IEEE Antennas and Wireless Propagation Letters*, Vol. 10, 1586–1589, 2011.
27. Murakami, Y., T. Hori, and M. Fujimoto, "Optimum reflector configuration for dipole antenna by using artificial magnetic conductor," *IEEE 2013 International Workshop on Antenna Technology (iWAT)*, 2013.
28. Simovski, C. R., P. de Maagt, and I. V. Melchakova, "High-impedance surfaces having stable resonance with respect to polarization and incidence angle," *IEEE Trans. Antennas and Propagation*, Vol. 53, No. 3, 908–914, 2005.